Constraints on Oscillation Parameters from ν_e Appearance and ν_μ Disappearance in NOvA

P. Adamson,[11] L. Aliaga,[11] D. Ambrose,[26] N. Anfimov,[22] A. Antoshkin,[22] E. Arrieta-Diaz,[31] K. Augsten,[9] A. Aurisano,[6] C. Backhouse,[4] M. Baird,[33,17] B. A. Bambah,[15] K. Bays,[4] B. Behera,[16] S. Bending,[37] R. Bernstein,[11] V. Bhatnagar,[27] B. Bhuyan,[13] J. Bian,[20,26] T. Blackburn,[33] A. Bolshakova,[22] C. Bromberg,[24] J. Brown,[26] G. Brunetti,[11] N. Buchanan,[8] A. Butkevich,[18] V. Bychkov,[26] M. Campbell,[37] E. Catano-Mur,[19] S. Childress,[11] B. C. Choudhary,[10] B. Chowdhury,[29] T. E. Coan,[31] J. A. B. Coelho,[36] M. Colo,[40] J. Cooper,[11] L. Corwin,[30] L. Cremonesi,[37] D. Cronin-Hennessy,[26] G. S. Davies,[17] J. P. Davies,[33] P. F. Derwent,[11] R. Dharmapalan,[1] P. Ding,[11] Z. Djurcic,[1] E. C. Dukes,[38] H. Duyang,[29] S. Edayath,[7] R. Ehrlich,[38] G. J. Feldman,[14] M. J. Frank,[28,38] M. Gabrielyan,[26] H. R. Gallagher,[36] S. Germani,[37] T. Ghosh,[12] A. Giri,[16] R. A. Gomes,[12] M. C. Goodman,[1] V. Grichine,[23] R. Group,[38] D. Grover,[3] B. Guo,[29] A. Habig,[25] J. Hartnell,[33] R. Hatcher,[11] A. Hatzikoutelis,[34] K. Heller,[26] A. Himmel,[11] A. Holin,[37] J. Hylen,[11] F. Jediny,[9] M. Judah,[8] G. K. Kafka,[14] D. Kalra,[27] S. M. S. Kasahara,[26] S. Kasetti,[15] R. Keloth,[7] L. Kolupaeva,[22] S. Kotelnikov,[23] I. Kourbanis,[11] A. Kreymer,[11] A. Kumar,[27] S. Kurbanov,[38] K. Lang,[35] W. M. Lee,[11,*] S. Lin,[8] J. Liu,[40] M. Lokajicek,[2] J. Lozier,[4] S. Luchuk,[18] K. Maan,[27] S. Magill,[1] W. A. Mann,[36] M. L. Marshak,[26] K. Matera,[11] V. Matveev,[18] D. P. Méndez,[33] M. D. Messier,[17] H. Meyer,[39] T. Miao,[11] W. H. Miller,[26] S. R. Mishra,[29] R. Mohanta,[15] A. Moren,[25] L. Mualem,[4] M. Muether,[39] S. Mufson,[17] R. Murphy,[17] J. Musser,[17] J. K. Nelson,[40] R. Nichol,[37] E. Niner,[17,11] A. Norman,[11] T. Nosek,[5] Y. Oksuzian,[38] A. Olshevskiy,[22] T. Olson,[36] J. Paley,[11] P. Pandey,[10] R. B. Patterson,[4] G. Pawloski,[26] D. Pershey,[4] O. Petrova,[22] R. Petti,[29] S. Phan-Budd,[41] R. K. Plunkett,[11] R. Poling,[26] B. Potukuchi,[21] C. Principato,[38] F. Psihas,[17] A. Radovic,[40] R. A. Rameika,[11] B. Rebel,[11] B. Reed,[30] D. Rocco,[26] P. Rojas,[8] V. Ryabov,[23] K. Sachdev,[11,26] P. Sail,[35] O. Samoylov,[22] M. C. Sanchez,[19] R. Schroeter,[14] J. Sepulveda-Quiroz,[19] P. Shanahan,[11] A. Sheshukov,[22] J. Singh,[27] J. Singh,[21] P. Singh,[10] V. Singh,[3] J. Smolik,[9] N. Solomey,[39] E. Song,[38] A. Sousa,[6] K. Soustruznik,[5] M. Strait,[26] L. Suter,[1,11] R. L. Talaga,[1] M. C. Tamsett,[33] P. Tas,[5] R. B. Thayyullathil,[7] J. Thomas,[37] X. Tian,[29] S. C. Tognini,[12] J. Tripathi,[27] A. Tsaris,[11] J. Urheim,[17] P. Vahle,[40] J. Vasel,[17] L. Vinton,[33] A. Vold,[26] T. Vrba,[9] B. Wang,[31] M. Wetstein,[19] D. Whittington,[17] S. G. Wojcicki,[32] J. Wolcott,[36] N. Yadav,[13] S. Yang,[6] J. Zalesak,[2] B. Zamorano,[33] and R. Zwaska[11]

(NOvA Collaboration)

[1]*Argonne National Laboratory, Argonne, Illinois 60439, USA*
[2]*Institute of Physics, The Czech Academy of Sciences, 182 21 Prague, Czech Republic*
[3]*Department of Physics, Institute of Science, Banaras Hindu University, Varanasi 221 005, India*
[4]*California Institute of Technology, Pasadena, California 91125, USA*
[5]*Charles University, Faculty of Mathematics and Physics, Institute of Particle and Nuclear Physics, 116 36 Prague, Czech Republic*
[6]*Department of Physics, University of Cincinnati, Cincinnati, Ohio 45221, USA*
[7]*Department of Physics, Cochin University of Science and Technology, Kochi 682 022, India*
[8]*Department of Physics, Colorado State University, Fort Collins, Colorado 80523-1875, USA*
[9]*Czech Technical University in Prague, Brehova 7, 115 19 Prague 1, Czech Republic*
[10]*Department of Physics and Astrophysics, University of Delhi, Delhi 110007, India*
[11]*Fermi National Accelerator Laboratory, Batavia, Illinois 60510, USA*
[12]*Instituto de Física, Universidade Federal de Goiás, Goiânia, Goiás 74690-900, Brazil*
[13]*Department of Physics, IIT Guwahati, Guwahati 781 039, India*
[14]*Department of Physics, Harvard University, Cambridge, Massachusetts 02138, USA*
[15]*School of Physics, University of Hyderabad, Hyderabad 500 046, India*
[16]*Department of Physics, IIT Hyderabad, Hyderabad 502 205, India*
[17]*Indiana University, Bloomington, Indiana 47405, USA*
[18]*Institute for Nuclear Research of Russia, Academy of Sciences 7a, 60th October Anniversary prospect, Moscow 117312, Russia*
[19]*Department of Physics and Astronomy, Iowa State University, Ames, Iowa 50011, USA*
[20]*Department of Physics and Astronomy, University of California at Irvine, Irvine, California 92697, USA*
[21]*Department of Physics and Electronics, University of Jammu, Jammu Tawi 180 006, Jammu and Kashmir, India*
[22]*Joint Institute for Nuclear Research, Dubna, Moscow region 141980, Russia*
[23]*Nuclear Physics Department, Lebedev Physical Institute, Leninsky Prospect 53, 119991 Moscow, Russia*
[24]*Department of Physics and Astronomy, Michigan State University, East Lansing, Michigan 48824, USA*
[25]*Department of Physics and Astronomy, University of Minnesota Duluth, Duluth, Minnesota 55812, USA*
[26]*School of Physics and Astronomy, University of Minnesota Twin Cities, Minneapolis, Minnesota 55455, USA*

[27]Department of Physics, Panjab University, Chandigarh 106 014, India
[28]Department of Physics, University of South Alabama, Mobile, Alabama 36688, USA
[29]Department of Physics and Astronomy, University of South Carolina, Columbia, South Carolina 29208, USA
[30]South Dakota School of Mines and Technology, Rapid City, South Dakota 57701, USA
[31]Department of Physics, Southern Methodist University, Dallas, Texas 75275, USA
[32]Department of Physics, Stanford University, Stanford, California 94305, USA
[33]Department of Physics and Astronomy, University of Sussex, Falmer, Brighton BN1 9QH, United Kingdom
[34]Department of Physics and Astronomy, University of Tennessee, Knoxville, Tennessee 37996, USA
[35]Department of Physics, University of Texas at Austin, Austin, Texas 78712, USA
[36]Department of Physics and Astronomy, Tufts University, Medford, Massachusetts 02155, USA
[37]Physics and Astronomy Department, University College London, Gower Street, London WC1E 6BT, United Kingdom
[38]Department of Physics, University of Virginia, Charlottesville, Virginia 22904, USA
[39]Department of Mathematics, Statistics, and Physics, Wichita State University, Wichita, Kansas 67206, USA
[40]Department of Physics, College of William & Mary, Williamsburg, Virginia 23187, USA
[41]Department of Physics, Winona State University, P.O. Box 5838, Winona, Minnesota 55987, USA

(Received 10 March 2017; revised manuscript received 9 May 2017; published 5 June 2017)

Results are reported from an improved measurement of $\nu_\mu \to \nu_e$ transitions by the NOvA experiment. Using an exposure equivalent to 6.05×10^{20} protons on target, 33 ν_e candidates are observed with a background of 8.2 ± 0.8 (syst.). Combined with the latest NOvA ν_μ disappearance data and external constraints from reactor experiments on $\sin^2 2\theta_{13}$, the hypothesis of inverted mass hierarchy with θ_{23} in the lower octant is disfavored at greater than 93% C.L. for all values of δ_{CP}.

DOI: 10.1103/PhysRevLett.118.231801

This Letter reports updated results on the rate of $\nu_\mu \to \nu_e$ transitions in the NOvA experiment [1] and constraints on oscillation parameters from the first combined fit of ν_e appearance and ν_μ disappearance data. The measurement, also probed by the MINOS (Main Injector Neutrino Oscillation Search) [2] and T2K (Tokai to Kamioka) [3] experiments, is sensitive to three unknowns in neutrino physics: the octant of θ_{23} (whether θ_{23} is less than, equal to, or greater than $\pi/4$), the neutrino mass hierarchy, and the amount of CP violation in the lepton sector. At the baseline and neutrino energy range of the NOvA experiment, the probability for ν_μ to oscillate to ν_e is primarily proportional to the combination $\sin^2\theta_{23}\sin^2 2\theta_{13}$. The disappearance of muon neutrinos is sensitive to the mixing angle θ_{23}, which is relatively weakly constrained to be near maximal ($\sin^2\theta_{23} \approx 0.5$) [2–4]. Reactor neutrino measurements tightly constrain $\sin^2 2\theta_{13}$ at 0.085 ± 0.005 [5–7]. The coherent forward scattering of the neutrino beam with electrons in the Earth enhances the electron neutrino appearance probability in the case of normal mass hierarchy (NH), where $\Delta m^2_{32} > 0$, and suppresses it for inverted mass hierarchy (IH), where $\Delta m^2_{32} < 0$. The possible violation of CP symmetry in the lepton sector is parameterized by δ_{CP}. CP-conserving oscillations occur if $\delta_{CP} = 0$ or π, while ν_e appearance is enhanced around $\delta_{CP} = 3\pi/2$ and suppressed around $\delta_{CP} = \pi/2$. At NOvA's energy and baseline, the impact of these three factors on the ν_e appearance probability are of similar magnitudes, which can lead to degeneracies between them, particularly when analyzing oscillations in neutrinos alone. For antineutrinos, the mass hierarchy and CP phase have the opposite effect on the oscillation probability, while increasing values of $\sin^2\theta_{23}$ increase the appearance probabilities for ν_e and $\bar{\nu}_e$ alike.

NOvA [8] observes neutrinos produced in Fermilab's NuMI [9] beam line in two detectors. The Far Detector (FD) is located on the surface, 14.6 mrad off the central beam axis, 810 km from the neutrino parent production source. The Near Detector (ND) is located 100 m underground, 1 km from the source, and measures the neutrino beam spectrum before oscillations occur. It is positioned to maximize the overlap between the neutrino energy spectra observed at the two detectors. At these locations, the beam is peaked around 2 GeV with neutrino energies mainly in the 1–3 GeV range. According to simulations, the neutrino beam at the ND is predominantly ν_μ, with 1.8% $\bar{\nu}_\mu$ and 0.7% $\nu_e + \bar{\nu}_e$ components for neutrino energies between 1 and 3 GeV.

The two functionally equivalent detectors [1,4,8,10] are constructed from planes of extruded polyvinyl chloride (PVC) cells [11]. The cells have a rectangular cross section measuring 3.9 cm by 6.6 cm and are 15.5 m (3.9 m) long in the FD (ND). Planes alternate the long cell dimension between vertical and horizontal orientations perpendicular to the beam. Each cell is filled with liquid scintillator [12]. Light is collected by a loop of wavelength-shifting fiber inside the cell. The fiber ends terminate on a single pixel of an avalanche photodiode (APD) [13]. The FD (ND) has a total active mass of 14 kt (193 t). In the fiducial region, the detectors are 62% scintillator by mass.

The data analyzed were collected between February 6, 2014 and May 2, 2016. The exposure is equivalent to 6.05×10^{20} protons on target (POT) collected in the full detector and corresponds to more than double the exposure used in previous results [1,4]. The fiducial mass for the full detector is 10.3 kt. The average neutrino beam power increased from 250 to 560 kW during the data-taking period.

Measuring the rate of electron-neutrino appearance requires the identification of charged-current (CC) interactions of ν_e and understanding the various backgrounds that are also selected at the FD. The signature of ν_e CC interactions in the NOvA detectors is an electromagnetic shower plus any associated hadronic recoil energy. The largest background arises from neutral current (NC) interactions of beam neutrinos that produce π^0 which decay to photons that mimic the signature of an electron. The intrinsic ν_e component of the NuMI beam represents an irreducible background to this search. Charged-current interactions of ν_μ with a short muon track and a hadronic shower with some electromagnetic activity comprise a smaller background. Other small backgrounds include cosmic-ray-induced events, particularly where a photon or a neutron enters from the sides of the detector, and charged-current interactions of ν_τ, which mostly occur above 3 GeV.

For this analysis, a new ν_e CC classifier was developed to select a signal sample with improved purity and efficiency. The convolutional visual network (CVN) [14] is a convolutional neural network and was designed using deep learning techniques from the field of computer vision [15,16]. Recorded hits in the detectors are formed into clusters by grouping hits in time and space to isolate individual interactions [17,18]. The CVN classifier takes the hits from these clusters, without any further reconstruction, as input and applies a series of trained linear operations to extract complex, abstract classifying features from the image. A multilayer perceptron [19,20] at the end of the network uses these features to create the classifier output. Training is conducted using a mixture of simulated FD ν_μ CC, ν_e CC, ν_τ CC, and NC events as well as a sample of FD cosmic data.

The NOvA simulation chain uses FLUKA [21], GEANT4 [22], FLUGG [23], GENIE [24], and a custom detector simulation [25] to model neutrino production in the beam line and subsequent interaction in the detector. Neutrino scattering off substructure in the nucleus is added to the simulation using an empirical model of multinucleon excitations and long-range correlations [26–29]. The implementation of this model in the NOvA simulation is tuned to match an observed excess of events in data over simulation in bins of reconstructed three-momentum transfer [30]. Additionally, the rate of nonresonant single pion production in charged-current interactions is effectively reduced by 50%, motivated by a recent reanalysis of ν_μ-deuterium pion-production data [31,32].

For the purpose of energy reconstruction and event containment, the event cluster is further reconstructed to determine particle paths. A Hough transform is applied to the cluster to identify global features, characterized as Hough lines [33]. The intersections of these lines seed an algorithm to produce a three-dimensional vertex for the cluster [34]. In both the horizontal and vertical detector views, hits are grouped into prongs radiating from the vertex [35,36]. Prongs are then matched between the views based on energy deposition characteristics.

The energy responses of the detectors are calibrated using minimum ionizing energy deposits in a region 1–2 m from the end of tracks corresponding to stopping cosmic ray muons. To reconstruct the electron neutrino candidate energy, the prong with the most calorimetric energy is assumed to be an electromagnetic shower caused by the outgoing electron. The remaining energy deposits in the event are attributed to the hadronic recoil system. The reconstructed ν_e energy is taken as a quadratic function of the electromagnetic and hadronic calorimetric responses. The function is a parameterization of the simulated true electron neutrino energy in relation to these quantities and yields an energy resolution of $\sim$7% in both detectors.

To suppress the cosmic-ray-induced background in the FD, selected events are required to be in a 12 μs window centered on the 10 μs beam spill. A large fraction of cosmic events deposit energy close to the detector edges and are removed due to containment requirements. Requiring a small reconstructed transverse momentum fraction with respect to the beam direction rejects cosmic events with angles too steep to be consistent with a NuMI beam event. The cosmic background rejection criteria are tuned using neutrino beam simulation and a large sample of cosmic data recorded asynchronously with the neutrino beam.

The maximum of the ν_e appearance signal is expected just below the peak neutrino energy at NOvA. Restricting the energy range of selected events to 1–3 GeV removes a large fraction of the NC and cosmic backgrounds, which are predominately of lower reconstructed energy, and intrinsic ν_e CC events, which dominate at higher energies. We similarly constrain the length of the longest track and number of hits in an event to remove clear muon tracks or poorly reconstructed events. Other than containment requirements, the ν_e CC selection criteria in the ND are very similar to those in the FD.

The selection criteria are chosen to maximize the figure of merit defined as $S/\sqrt{S+B}$, where S and B are the number of signal and background events, respectively. The final ν_e selection criteria select a contained appearance signal with 73.5% efficiency and 75.5% purity, representing a gain in sensitivity of 30% compared to the ν_e classifiers used in the previously reported results [1]. These criteria also reject 97.6% of the NC and 99.0% of the ν_μ CC beam backgrounds. The cosmic ray backgrounds are suppressed by 7 orders of magnitude, and only 0.53 ± 0.14 cosmic events are estimated to be selected in the final ν_e appearance sample based on the performance of ν_e selection criteria on cosmic data. Of the beam backgrounds that pass all ν_e selection, 91% contain some form of energetic electromagnetic shower. To further improve the statistical power of this analysis, events selected in the FD are split into three ν_e classifier bins, containing signal ν_e CC events with low, medium, and high purity. The analysis is performed in four energy bins between 1 and 3 GeV for each of the three classifier bins.

The ND has a negligible ν_e appearance signal and is used to estimate the beam-neutrino-induced background rates to the appearance measurement. According to the simulation, the kinematics of the events that pass the ν_e CC selection criteria in the ND are representative of and adequately cover those selected in the FD. Figure 1 shows that there is an overall ∼10% excess of data over the simulation in the ν_e CC selected events in the ND. Since the NC, ν_μ CC, and beam ν_e CC background components are affected differently by oscillations, the total background selected in the ND data is broken down into these components, which are then used to estimate the corresponding components in the FD.

Both the ν_μ and intrinsic ν_e components of the beam peak arise primarily from pions decaying through the process ($\pi^+ \to \mu^+ + \nu_\mu$) as well as the subsequent muon decay ($\mu^+ \to e^+ + \bar{\nu}_\mu + \nu_e$). At higher energies, they originate from kaon decays. The pion and kaon hadron yields can be derived from the low- and high-energy ν_μ CC rate in the ND data and are used to correct the ν_e CC rate in the simulation. Pion yields are adjusted in bins of transverse and longitudinal pion momentum, while the kaon yield is simply scaled. From this method, it is inferred that the kaon yield is higher by 17% and the pion yield lower by 3% than predicted by the simulation. This results in an overall 1% increase in the estimated intrinsic ν_e CC background rate in the 1–3 GeV range in the ND.

Some of the ν_μ CC interactions that are a background to the ν_e CC selection have a muon hidden in the shower associated with the hadronic recoil. In these events, the

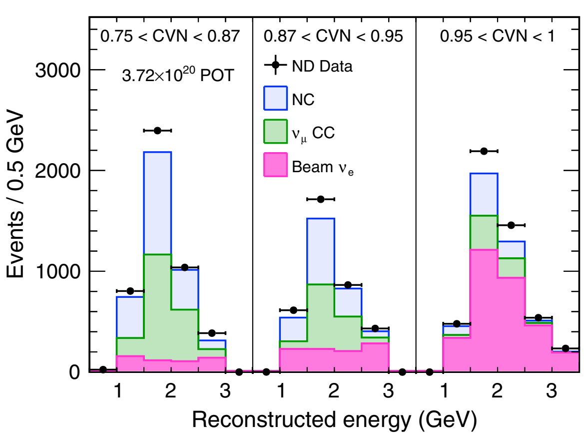

FIG. 1. Reconstructed energy of events selected in the ND data and simulation by the ν_e CC selection criteria in the three ν_e classifier (CVN) bins. The leftmost panel is the lowest purity classifier bin, while the rightmost has the highest purity.

time-delayed electron from muon decay (Michel electron) may often be found. The hadronic recoil system also produces this signature due to the presence of charged pions that decay to muons. However, on average, ν_μ CC interactions have one more Michel electron than ν_e CC and NC interactions. The ν_μ CC and NC background components are varied in each bin of energy and ν_e classifier to obtain the best match to the distribution of the number of Michel electron candidates in the data. The intrinsic ν_e CC background component is held fixed at the value obtained from the pion and kaon yield analysis. This method leads to an integrated increase of 17.7% and 10.4% in the ν_μ CC and NC background rates, respectively, relative to those predicted by the ND simulation. These corrections derived from the ND data account for the 10% discrepancy with the simulation and are applied to the background spectra in the FD simulation in the analysis bins. The spectra are then weighted by the appropriate three-flavor oscillation probability to obtain the final estimates of the beam backgrounds in the FD. After applying these data-driven constraints, the predicted background composition in the FD for this analysis is 45.3% NC, 38% intrinsic ν_e CC, 8.4% ν_μ CC, 1.8% ν_τ CC, and 6.5% cosmic events.

The ν_e appearance signal expected in the FD is also constrained by the observed neutrino beam spectrum in the ND. A sample of ν_μ candidates are selected in the ND data using the latest ν_μ selection criteria as described in Ref. [30], and the underlying true energy spectrum is derived from a reconstructed to true energy migration matrix. The spectrum of true ν_e CC signal events selected in the FD simulation is corrected by the ratio of the ν_μ CC true energy spectrum derived from ND data to the simulated ν_μ CC spectrum. The adjusted FD signal spectrum is weighted by the ν_e appearance probability and mapped back to the reconstructed energy spectrum for the final estimate of the ν_e appearance signal. This extrapolation is carried out for the energy spectra in all three ν_e classifier bins. Figure 2 shows the variation in the number of FD events predicted as a function of the assumed oscillation parameters.

The ND data are also used to verify the simulated ν_e CC selection efficiency. For events that pass the ν_μ CC selection criteria in the ND data and simulation, the energy deposits along the reconstructed track of the candidate muon are removed [37]. An electron with the same energy and direction is simulated in its place to construct ν_e CC-like interactions in both the data and simulation. The event is reconstructed again with the electron shower embedded in it, and the ν_e selection cuts are applied. The efficiency of the ν_e CC selection criteria in the ND between the data and simulation for identifying neutrino events with inserted electrons matches to within 1%.

Systematic uncertainties are evaluated by reweighting or generating new simulated event samples modified to account for each uncertainty in the ND and FD. The full

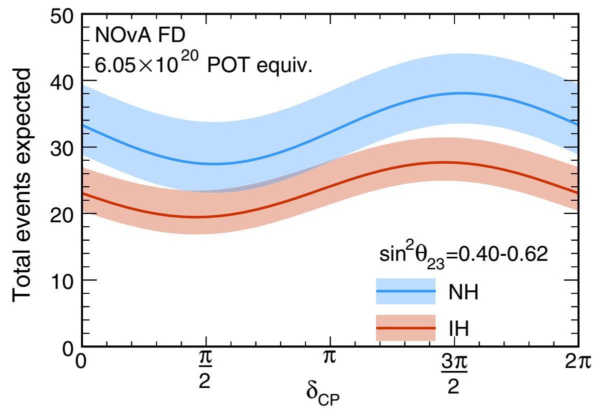

FIG. 2. Total number of selected ν_e candidate events expected at the FD. The blue represents NH and the orange IH. The bands correspond to the range $\sin^2\theta_{23} = 0.40$ (lower edge) to 0.62 (upper edge), with the solid line marking the maximal mixing. The x axis gives the value of the CP phase, while all other parameters are held fixed at the best-fit values found by NOvA's latest analysis of ν_μ disappearance [30].

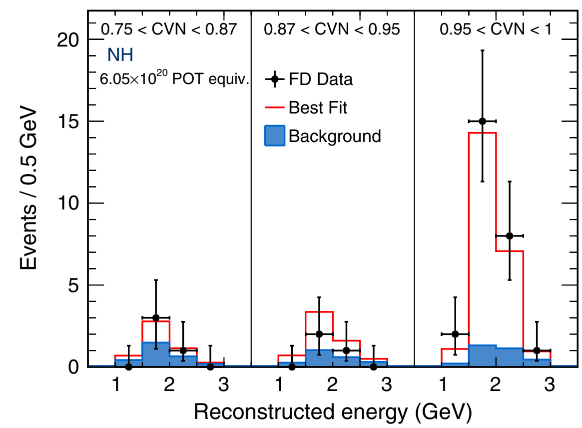

FIG. 3. Reconstructed energy of selected FD events in three bins of the CVN classifier variable. Black points show the data, and the red line shows the predicted spectrum at the best-fit point in NH, with the blue area showing the total expected background.

analysis, including a background component estimation in the ND data and extrapolation to FD, is performed with these systematically shifted simulation samples to predict the altered signal and background spectra at the FD. Calibration and normalization are the leading sources of systematic uncertainty for the background and signal, respectively. Other sources of systematic uncertainty considered include neutrino flux, modeling of neutrino interactions, and detector response. The overall effect of the uncertainties summed in quadrature on the total event count is 5.0% (10.5%) on the signal (background). The statistical uncertainties of 20.1% (34.9%) on the signal (background) therefore dominate.

After the event selection criteria and analysis procedures were finalized, an inspection of the FD data revealed 33 ν_e candidates, of which 8.2 ± 0.8 (syst.) events are predicted to be background [38]. Figure 3 shows a comparison of the event distribution with the expectations at the best-fit point as a function of the classifier variable and reconstructed neutrino energy.

To extract oscillation parameters, the ν_e CC energy spectrum in bins of event classifier is fit simultaneously with the FD ν_μ CC energy spectrum [30]. The NOvA ν_μ disappearance result constrains $\sin^2\theta_{23}$ around degenerate best-fit points of 0.404 and 0.624. The likelihood between the observed spectra and the Poisson expectation in each bin is computed as a function of the oscillation parameters $|\Delta m^2_{32}|$, θ_{23}, θ_{13}, δ_{CP}, and the mass hierarchy. Each source of systematic uncertainty is incorporated into the fit as a nuisance parameter, which varies the predicted FD spectrum according to the shifts determined from systematically shifted samples. Where systematic uncertainties are common between the two data sets, the nuisance parameters associated with the effect are correlated appropriately. Gaussian penalty terms are applied to represent the estimates of the 1σ ranges of these parameters and the knowledge of $\sin^2 2\theta_{13} = 0.085 \pm 0.005$ from reactor experiments [40].

Figure 4 shows the regions of $(\sin^2\theta_{23}, \delta_{CP})$ space allowed at various confidence levels. The likelihood surface

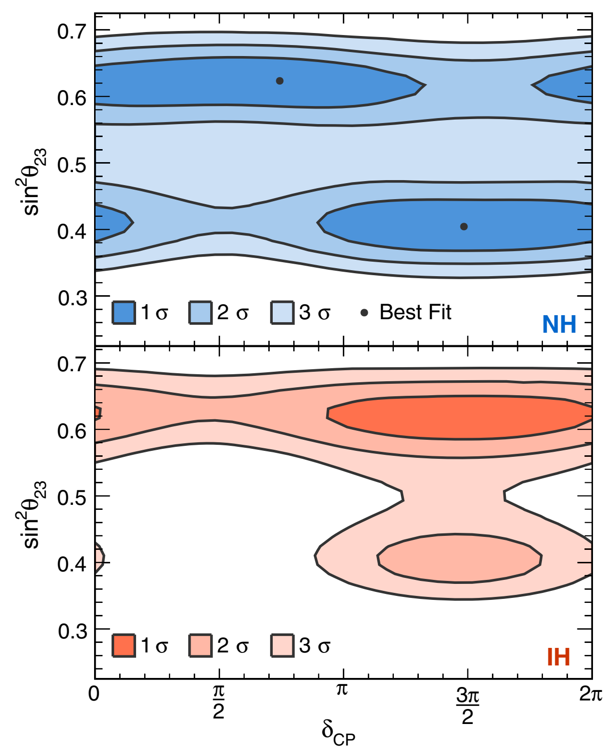

FIG. 4. Regions of δ_{CP} vs $\sin^2\theta_{23}$ parameter space consistent with the observed spectrum of ν_e candidates and the ν_μ disappearance data [30]. The top panel corresponds to normal mass hierarchy ($\Delta m^2_{32} > 0$) and the bottom panel to inverted hierarchy ($\Delta m^2_{32} < 0$). The color intensity indicates the confidence level at which particular parameter combinations are allowed.

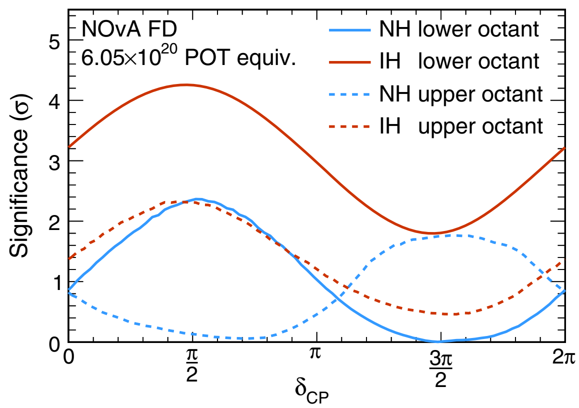

FIG. 5. Feldman-Cousins corrected significance at which each value of δ_{CP} is disfavored for each of the four possible combinations of mass hierarchy [normal (blue curves) or inverted (red curves)] and θ_{23} octant [lower (solid curves) or upper (dashed curves)] by the combination of ν_e appearance and NOvA's latest ν_μ disappearance measurement [30].

is profiled over the parameters $|\Delta m^2_{32}|$ and θ_{13}, while the solar parameters Δm^2_{21} and θ_{12} are held fixed. The significances are derived using the Feldman-Cousins unified approach [41] to account for the statistical effects of a low event count and physical boundaries.

Figure 5 shows the significance at which values of δ_{CP} are disfavored for each hierarchy and octant combination. The value of $\sin^2\theta_{23}$ is profiled within the specified octant. There are two degenerate best-fit points, both in the normal hierarchy: $\sin^2\theta_{23} = 0.404$, $\delta_{CP} = 1.48\pi$ and $\sin^2\theta_{23} = 0.623$, $\delta_{CP} = 0.74\pi$. The inverted hierarchy predicts fewer events than are observed for all values of δ_{CP} and both octants. The best-fit point in the inverted hierarchy occurs near $\delta_{CP} = 3\pi/2$ and is 0.46σ from the global best-fit points. The inverted mass hierarchy in the lower octant is disfavored at greater than 93% C.L. for all values of δ_{CP} and excluded at greater than 3σ significance outside the range $0.97\pi < \delta_{CP} < 1.94\pi$. The T2K Collaboration has recently published results based on their observation of ν_μ ($\bar{\nu}_\mu$) disappearance and ν_e ($\bar{\nu}_e$) appearance [42]. While their data favor a near-maximal value of θ_{23}, they disfavor CP conservation at 90% C.L., with a weak preference for normal mass hierarchy. These observations are broadly consistent with the NOvA result.

In conclusion, in the first combined fit of the NOvA ν_e appearance and ν_μ disappearance data, the inverted mass hierarchy with θ_{23} in the lower octant is disfavored at greater than 93% C.L. for all values of δ_{CP}. Future data-taking in antineutrino mode, where the impact of the mass hierarchy and CP phase are reversed with respect to their effect on neutrinos, will help resolve the remaining degeneracies in the parameters.

This work was supported by the U.S. Department of Energy; the U.S. National Science Foundation; the Department of Science and Technology, India; the European Research Council; the MSMT CR, GA UK, Czech Republic; the RAS, RMES, and RFBR, Russia; CNPq and FAPEG, Brazil; and the State and University of Minnesota. We are grateful for the contributions of the staffs at the University of Minnesota module assembly facility and Ash River Laboratory, Argonne National Laboratory, and Fermilab. Fermilab is operated by Fermi Research Alliance, LLC under Contract No. De-AC02-07CH11359 with the U.S. DOE.

*Deceased.

[1] P. Adamson *et al.*, Phys. Rev. Lett. **116**, 151806 (2016).
[2] P. Adamson *et al.*, Phys. Rev. Lett. **112**, 191801 (2014).
[3] K. Abe *et al.*, Phys. Rev. D **91**, 072010 (2015).
[4] P. Adamson *et al.*, Phys. Rev. D **93**, 051104 (2016).
[5] F. P. An *et al.*, Phys. Rev. Lett. **115**, 111802 (2015).
[6] S. B. Kim, Nucl. Phys. **B908**, 94 (2016).
[7] Y. Abe *et al.*, J. High Energy Phys. 01 (2016) 163.
[8] NOvA Technical Design Report No. FERMILAB-DESIGN-2007-01.
[9] P. Adamson *et al.*, Nucl. Instrum. Methods Phys. Res., Sect. A **806**, 279 (2016); NuMI Technical Design Handbook Report No. FERMILAB-DESIGN-1998-01.
[10] S. Magill, J. Phys. Conf. Ser. **404**, 012035 (2012); P. Border *et al.*, Nucl. Instrum. Methods Phys. Res., Sect. A **463**, 194 (2001).
[11] R. L. Talaga *et al.*, Report No. FERMILAB-PUB-15-049-ND-PPD.
[12] S. Mufson *et al.*, Nucl. Instrum. Methods Phys. Res., Sect. A **799**, 1 (2015).
[13] The NOvA APD is a custom variant of the Hamamatsu S8550. http://www.hamamatsu.com/us/en/product/alpha/S/4112/S8550-02/index.html.
[14] A. Aurisano, A. Radovic, D. Rocco, A. Himmel, M. D. Messier, E. Niner, G. Pawloski, F. Psihas, A. Sousa, and P. Vahle, J. Instrum. **11**, P09001 (2016).
[15] C. Szegedy *et al.*, arXiv:1409.4842.
[16] D. E. Rumelhart, G. E. Hinton, and R. J. Williams, Nature (London) **323**, 533 (1986).
[17] M. Baird, Ph.D. thesis, Indiana University, 2015.
[18] M. Ester *et al.*, in *Proceedings of the Second International Conference on Knowledge Discovery and Knowledge Engineering and Knowledge Management*, 1996 (unpublished).
[19] F. Rosenblatt, *Principles of Neurodynamics: Perceptrons and the Theory of Brain Mechanisms* (Spartan Books, Washington, 1961).
[20] R. Reed and R. Marks, *Neural Smithing: Supervised Learning in Feedforward Artificial Neural Networks*, a Bradford book (MIT Press, Cambridge, MA, 1999).
[21] T. T. Böhlen, F. Cerutti, M. P. W. Chin, A. Fassò, A. Ferrari, P. G. Ortega, A. Mairani, P. R. Sala, G. Smirnov, and V. Vlachoudis, Nucl. Data Sheets **120**, 211 (2014); A. Ferrari *et al.*, Technical Report No. CERN-2005-010, 2005.
[22] S. Agostinelli *et al.*, Nucl. Instrum. Methods Phys. Res., Sect. A **506**, 250 (2003); J. Allison *et al.*, IEEE Trans. Nucl. Sci. **53**, 270 (2006).
[23] M. Campanella *et al.*, Technical Report No. CERN-ATL-SOFT-99-004, 1999.

[24] C. Andreopoulos *et al.*, Nucl. Instrum. Methods Phys. Res., Sect. A **614**, 87 (2010); C. Andreopoulos *et al.*, arXiv: 1510.05494.

[25] A. Aurisano, C. Backhouse, R. Hatcher, N. Mayer, J. Musser, R. Patterson, R. Schroeter, and A. Sousa, J. Phys. Conf. Ser. **664**, 072002 (2015).

[26] M. Martini and M. Ericson, Phys. Rev. C **87**, 065501 (2013).

[27] R. Gran, J. Nieves, F. Sanchez, and M. J. Vicente Vacas, Phys. Rev. D **88**, 113007 (2013).

[28] G. D. Megias *et al.*, Phys. Rev. D **91**, 073004 (2015).

[29] O. Lalakulich, K. Gallmeister, and U. Mosel, Phys. Rev. C **86**, 014614 (2012); **90**, 029902(E) (2014).

[30] P. Adamson *et al.*, Phys. Rev. Lett. **118**, 151802 (2017).

[31] C. Wilkinson, P. Rodrigues, S. Cartwright, L. Thompson, and K. McFarland, Phys. Rev. D **90**, 112017 (2014).

[32] P. Rodrigues, C. Wilkinson, and K. McFarland, Eur. Phys. J. C **76**, 474 (2016).

[33] L. Fernandes and M. Oliveira, Pattern Recognit. **41**, 299 (2008).

[34] M. Gyulassy and M. Harlander, Comput. Phys. Commun. **66**, 31 (1991); M. Ohlsson and C. Peterson, Comput. Phys. Commun. **71**, 77 (1992); M. Ohlsson, Comput. Phys. Commun. **77**, 19 (1993); R Frühwirth and A. Strandlie, Comput. Phys. Commun. **120**, 197 (1999).

[35] R. Krishnapuram and J. M. Keller, IEEE Transactions on Fuzzy Systems **1**, 98 (1993); M. S. Yang and K. L. Wu, Pattern Recognit. **39**, 5 (2006).

[36] E. Niner, Ph.D. thesis, Indiana University, 2015.

[37] K. Sachdev, Ph.D. thesis, University of Minnesota, 2015.

[38] The backgrounds are computed at the best-fit oscillation parameters: $\sin^2\theta_{23} = 0.40$, $\sin^2 2\theta_{13} = 0.085$, $\Delta m^2_{32} = 2.67\times10^{-3}\,\mathrm{eV}^2$, and $\delta_{CP} = 1.48\pi$. The matter density, computed for the average depth of the NuMI beam in Earth's crust for the NOvA baseline of 810 km using the CRUST2.0 [39] model, is $2.84\ \mathrm{g/cm}^3$.

[39] G. Laske, C. Bassin, and G. Masters, EOS Trans. AGUF **897**, 81 (2000).

[40] K. A. Olive *et al.* (Particle Data Group), Chin. Phys. C **38**, 090001 (2014), and 2015 update.

[41] G. J. Feldman and R. D. Cousins, Phys. Rev. D **57**, 3873 (1998).

[42] K. Abe *et al.*, Phys. Rev. Lett. **118**, 151801 (2017).